NeuroImage 81 (2013) 178–190

Contents lists available at SciVerse ScienceDirect

NeuroImage

journal homepage: www.elsevier.com/locate/ynimg

Heart cycle-related effects on event-related potentials, spectral power changes, and connectivity patterns in the human ECoG

Markus Kern [a,b], Ad Aertsen [a,c], Andreas Schulze-Bonhage [b,c], Tonio Ball [b,c,*]

[a] Neurobiology and Biophysics, Faculty of Biology, University of Freiburg, Schänzlestrasse 1, 79104 Freiburg, Germany
[b] Epilepsy Center, University Medical Center Freiburg, Breisacher Straße 64, 79106 Freiburg, Germany
[c] Bernstein Center Freiburg, University of Freiburg, Hansastr. 9A, 79104 Freiburg, Germany

ARTICLE INFO

Article history:
Accepted 3 May 2013
Available online 16 May 2013

Keywords:
Heartbeat-evoked potential
Somatosensory cortex
Electrocorticogram
Phase synchrony
Connectivity
Signal quality

ABSTRACT

The perception of one's own heartbeat is a fundamental interoceptive process that involves cortical and subcortical structures. Yet, the precise spatiotemporal neuronal activity patterns underlying the cortical information processing have remained largely elusive. Although the high temporal and spatial resolution of electrocorticographic (ECoG) recordings is increasingly being exploited in functional neuroimaging, it has not been used to study heart cycle-related effects. Here, we addressed the capacity of ECoG to characterize neuronal signals within the cardiac cycle, as well as to disentangle them from heart cycle-related artifacts. Based on topographical distribution and latency, we identified a biphasic potential within the primary somatosensory cortex, which likely constitutes a heartbeat-evoked potential (HEP) of neuronal origin. We also found two different types of artifacts: i) oscillatory potential changes with a frequency identical to the heart pulse rate, which probably represent pulsatility artifacts and ii) sharp potentials synchronized to the R-peak, corresponding to the onset of ventricular contraction and the cardiac field artifact (CFA) in EEG. Finally, we show that heart cycle-related effects induce pronounced phase-synchrony patterns in the ECoG and that this kind of correlation patterns, which may confound ECoG connectivity studies, can be reduced by a suitable correction algorithm. The present study is, to our knowledge, the first one to show a focally localized cortical HEP that could be clearly and consistently observed over subjects, suggesting a basic role of primary sensory cortex in processing of heart-related sensory inputs. We also conclude that taking into account and reducing heart cycle-related effects may be advantageous for many ECoG studies, and are of crucial importance, particularly for ECoG-based connectivity studies. Thus, in summary, although ECoG poses new challenges, it opens up new possibilities for the investigation of heartbeat-related viscerosensory processing in the human brain.

© 2013 Elsevier Inc. All rights reserved.

Introduction

The investigation of heart cycle-related brain activity in the context of conscious perception of one's own heartbeat has become a prominent topic in recent years (Bechara and Naqvi, 2004; Critchley et al., 2004; Khalsa et al., 2009; Pollatos et al., 2007; Tracy et al., 2007). Heartbeat-evoked potentials (HEPs) have been frequently investigated with EEG (Dirlich et al., 1998; Fukushima et al., 2011; Gray et al., 2007; Leopold and Schandry, 2001; Montoya et al., 1993; Pérez et al., 2005; Pollatos and Schandry, 2004; Pollatos et al., 2005; Schandry and Montoya, 1996; Schandry and Weitkunat, 1990; Schandry et al., 1986; Shao et al., 2011; Yuan et al., 2007) and were found to be modulated by psychological factors such as attention, motivation and the ability to consciously perceive heartbeats. Sources of the reported HEPs that were frequently discussed include the somatosensory and frontal cortex (Dirlich et al., 1998; Leopold and Schandry, 2001; Montoya et al., 1993; Pollatos and Schandry, 2004; Schandry and Weitkunat, 1990; Schandry et al., 1986) as well as cingulate and insular regions (Cameron and Minoshima, 2002; Critchley et al., 2004; Khalsa et al., 2009; Pollatos et al., 2005). Different latencies of the HEP were reported, ranging from 200 ms to 650 ms relative to the ECG-R-peak (Tables 1 and 2). The exact time-course of the HEP, however, was difficult to determine with the EEG because of the low EEG signal-to-noise ratio (SNR) during the time segment from the R-peak of the ECG signal until the complete decay of the T wave (Dirlich et al., 1997). This low SNR results from a heart cycle-related artifact termed the cardiac field artifact (CFA) which contaminates EEG recordings. The CFA is thought to originate from the myocardial muscle and can be measured anywhere on the body surface, including the scalp, where it is prominently seen in the EEG. The

Abbreviations: CFA, cardiac field artifact; CSF, cerebrospinal fluid; ECoG, electrocorticogram; EEG, electroencephalogram; EMG, electromyogram; ESM, electrical stimulation mapping; FDR, false discovery rate; HEP, heartbeat-evoked potential; PSI, phase synchrony index; SNR, signal-to-noise-ratio.

* Corresponding author at: Department of Neurosurgery, Epilepsy Center, University Medical Center Freiburg, Engelbergerstr. 21, D-79106 Freiburg im Breisgau, Germany.
E-mail address: tonio.ball@uniklinik-freiburg.de (T. Ball).

1053-8119/$ – see front matter © 2013 Elsevier Inc. All rights reserved.
http://dx.doi.org/10.1016/j.neuroimage.2013.05.042

Table 1
Types of heart cycle-related effects in the EEG.

	Heartbeat-evoked potential (HEP)	Cardiac field artifact (CFA)	Pulsatility artifacts due to pulsating blood vessels
Timing	Potential changes in the time interval 200 ms to 650 ms relative to the R-peak of the ECG signal. Exact time course unclear.	Sharp peak at the R-peak. Time course resembles the time course of the ECG during the QRST-complex	Peaks ~200 ms relative to the R-peak of the ECG signal. Smooth-wave- or saw-tooth-like time course with the same frequency as the pulse rate.
Spatial distribution	Regional occurrence in frontal, central and parietal EEG channels	Global occurrence in all/most EEG channels	Local occurrence in EEG channels near blood vessels

Timing and spatial distribution in the EEG as described in previous studies.

typical feature of the CFA in EEG recordings is a sharp potential peaking at the time point of the ECG R-peak (Schandry et al., 1986).

A third kind of heart cycle-related effects is pulsatility artifacts. These include artifacts originating from pulsating blood vessels, from pulsatile circulation of the cerebrospinal fluid (CSF) and from the resulting pulsatile motion of brain tissue. In EEG recordings, for example, the placing of electrodes on or near an artery is usually avoided, because pulsatility artifacts can be caused by the contraction and expansion of the blood vessel. Pulsatility artifacts in the EEG can appear with pulse-synchronous smooth wave- (Binnie, 2003; Dworetzky et al., 2010; Hirsch and Brenner, 2010; Stern, 2004) or saw-tooth-like (Cooper et al., 2003b; Zumsteg et al., 2004) time course. Corresponding artifact peaks were reported to appear invariably at ~200 ms after the ECG R-peak (Hirsch and Brenner, 2010; Zumsteg et al., 2004). In ECoG recordings, such pulse-related movement of electrode contacts due to nearby pulsating blood vessels may contribute artifact components to the recorded signals, especially in low frequencies, as suggested by Bleichner et al. (2011). Regarding the origin of pulsatile circulation of CSF, it was proposed that the change of internal pressure in the arteries during the systolic phase of the heart cycle results in an expansion of the vessel diameter which propagates into the CSF. The resulting intracranial pressure wave starts in the frontal lobe and moves into the more posterior parts of the brain, thus causing a motion of brain tissue (Enzmann and Pelc, 1992; Greitz et al., 1992; Wagshul et al., 2011). It has been proposed that this intracranial pressure wave and the resulting pulsatile motion of CSF and brain tissue may also have an impact on scalp EEG signals (Dirlich et al., 1998; Schroth and Klose, 1992a,b) and might be a source of ECoG pulsatility artifacts, as well. Characteristics of these three types of heart cycle-related effects (HEPs, CFA, and pulsatility artifacts) in EEG recordings are summarized in Table 1.

To our knowledge, systematic investigations of heart cycle-related effects in the ECoG, irrespective of whether they present bio-electrical artifacts or heart cycle-related brain activity, are lacking. ECoG recordings obtained from electrodes placed directly on the surface of the brain have advantages over non-invasive EEG recordings, including higher spatial and temporal accuracy (Engel et al., 2005), decreased susceptibility to artifact contamination and, hence, better overall signal quality (Ball et al., 2009a). Until recently, it was often assumed that major artifacts are absent in ECoG, although no quantitative investigations on the signal properties and limitations of ECoG recordings were available. In recent years, however, ocular artifacts, including eye-blink artifacts (Ball et al., 2009a) and saccade-related ocular EMG (Kovach et al., 2011) as well as chewing artifacts (Shimoda et al., 2012) were investigated in the ECoG. The proximity of blood vessels to the implanted electrode contacts was identified to be one of the most important causes of anomalous signals (Miller et al., 2009) and presumed to be the cause of the main artifact (i.e., the pulse related artifact) in ECoG recordings (Panagiotides et al., 2011). Pulsatility artifacts due to pulsating brain tissue could also contaminate ECoG recordings, given that brain pulsations are clearly visible with each heartbeat when the brain is exposed (Handy, 2004). It is, however, still unknown to what degree the different heart cycle-related effects known from EEG are present in ECoG recordings. For example, it remains unclear whether the skull insulates sufficiently to shield the brain (and ECoG recordings) from CFA contamination, and whether blood vessels can act as low conductance pathways through which the CFA may "tunnel" into the intracranial cavity.

Clarification of the role of heart cycle-related effects in the ECoG is important for several reasons. For example, to study heart cycle-related neuronal processing with ECoG, it is necessary to reliably distinguish neuronal signal components from others in the ECoG. As another example, variability induced by heart cycle-related effects in ECoG could lead to alterations of functional connectivity maps, comparable to the consequences of pulsatility artifacts in functional magnetic resonance imaging (fMRI), where it was argued that changes in pulse rate can significantly alter the results of functional connectivity analyses (Chang et al., 2009). Similarly, in the ECoG, pulsatility-artifact-evoked phase synchrony or changes in other connectivity measures could be misinterpreted as indexing neural functional connectivity.

The aim of the present study was to characterize heart cycle-related effects in ECoG recordings. Based on the EEG literature, we expected (i) HEPs in the time range from 200 ms to 650 ms relative to the ECG R-peak, located over the somatosensory and/or frontal cortex and/or cingulate/insular regions; (ii) the CFA, most prominently during the QRS complex and to a lesser extent during the T wave; and (iii) pulsatility artifacts with a smooth wave- or saw-tooth-like time course, with the same frequency as the pulse rate and with higher amplitudes than in the EEG, due to the greater proximity of the ECoG electrodes especially to blood vessels. In addition to potentials in the time domain, we were also interested in effects in the time–frequency domain because heart cycle-related spectral power modulations of ECoG activity had, to our knowledge, not yet been analyzed with electrophysiological recordings. Yet, at the same time, many previous ECoG studies rely on time–frequency representations of ECoG activity (Ball et al., 2008; Crone et al., 1998a,b, 2006; Lachaux et al., 2005; Pistohl et al., 2012; Schalk et al., 2008; Sinai et al., 2005). Finally, we evaluated a template correction approach to avoid heart cycle-related phase-synchrony patterns in the ECoG.

Materials and methods

Patients and data collection

Data sets from five patients undergoing evaluation for epilepsy surgery were used for the analysis of heart pulse-related ECoG changes. Sex, age and diagnosed anatomical pathologies of these patients were: Patient 1 (P1): female, 17 years, focal cortical dysplasia in the left fronto-polar cortex; patient 2 (P2): male, 17 years, focal cortical dysplasia in the left prefrontal cortex; patient 3 (P3): female, 16 years, focal cortical dysplasia in the right premotor–prefrontal cortex; patient 4 (P4) male, 47 years, focal cortical dysplasia right occipital-lateral cortex; patient 5 (P5) female, 26 years, dysplasia in the left temporal lobe; and patient 6 (P6) male, 19 years, dysplasia in the left prefrontal cortex. Written informed consent was obtained from all patients, stating that the electrophysiological data obtained during the diagnostic process might be used for scientific purposes.

The ECoG was recorded with subdurally-implanted grid- and strip-electrodes using a clinical AC EEG-System (IT-Med, Germany) with sampling rates of 256 Hz (P1, P2 and P3) and 1024 Hz (P4). Recordings were hardware high-pass filtered with a 0.032-Hz cutoff

Table 2
Previous EEG studies on heartbeat-evoked potentials (HEPs).

Title	Authors and date of publication	HEP location	HEP latency (ms)
From the heart to the brain: a study of heartbeat contingent scalp potentials	Schandry et al. (1986)	Frontal regions	250–400
Enhancement of heartbeat-related brain potentials through cardiac awareness training	Schandry and Weitkunat (1990)	Frontal regions	250–400
Heartbeat evoked potentials (HEPs): topography and influence of cardiac awareness and focus of attention	Montoya et al. (1993)	Frontal regions	350–550
Topography and morphology of heart action-related EEG potentials	Dirlich et al. (1998)	Parietal regions	350–650
The heartbeat-evoked brain potential in patients suffering from diabetic neuropathy and in healthy control persons	Leopold and Schandry (2001)	Frontal, central and temporal regions	280–330
Accuracy of heartbeat perception is reflected in the amplitude of the heartbeat-evoked brain potential	Pollatos and Schandry (2004)	Fronto-central regions	250–350
Suppression of the cardiac electric field artifact from the heart action evoked potential	Pérez et al. (2005)	Not specified	200–400
Brain structures involved in interoceptive awareness and cardioafferent signal processing: a dipole source localization study	Pollatos et al. (2005)	Anterior cingulate cortex, right insula, prefrontal cortex and left secondary somatosensory cortex	250–450
A cortical potential reflecting cardiac function	Gray et al. (2007)	Left temporal and lateral frontal regions	455–595
Effect of heartbeat perception on heartbeat evoked potential waves	Yuan et al. (2007)	Frontal and central regions	250–450
Association between interoception and empathy: evidence from heartbeat-evoked brain potential	Fukushima et al. (2011)	Fronto-central regions	250–430
Effect of pain perception on the heartbeat evoked potential	Shao et al. (2011)	Fronto-central regions	200–600

Studies are sorted according to their publication date. HEP latencies are relative to the ECG R-peak.

frequency and low-pass filtered approx. at 100 Hz (P1, P2 and P3) and at 400 Hz (P4). For P5 and P6, the ECoG was recorded with the same type of electrodes but using another amplifier (clinical Neuvo amplifier) with a sampling rate of 2000 Hz.

To map sensory and/or motor responses, electrical stimulation mapping (ESM) through the electrode grid was performed using an INOMED NS 60 stimulator (INOMED, Germany). Trains of 7-s duration consisted of 50 Hz pulses of alternating polarity square waves of 200 μs each. The intensity of stimulation was gradually increased, typically up to 15 mA or to the induction of sensory and/or motor phenomena, whichever occurred first. Patients were unaware of the timing of stimulation, unless motor or sensory symptoms were evoked. The positions of the implanted electrodes were determined from a structural T1 weighted MRI scan of 1 mm isotropic resolution obtained while the electrodes were implanted. This MRI data set was normalized to MNI space using SMP5 to obtain MNI coordinates of the implanted electrodes and to enable inter-subject comparison.

We used intra-operatively-acquired photographs before and after electrode implantation of two patients (P5 and P6) to address the question how subdural blood vessels are related to the CFA and pulsatility artifacts in ECoG recordings.

For the present study, we used heartbeats from recordings of patients during natural behavior, i.e., the patients were neither instructed to attempt to consciously perceive their heartbeats nor to ignore the perception. The numbers of trials obtained (for the algorithm used for R-peak detection, see below) were: P1 2270 heartbeats; P2 6449 heartbeats; P3 7263 heartbeats; P4 2802 heartbeats; P5 2661 heartbeats; and P6 5980 heartbeats. Thus, by using heartbeats during natural behavior, large numbers of trials could be achieved without additional burden on the patients.

Pre-processing and R-peak detection

As a first step of data analysis, we re-referenced the ECoG to a common average (CA) reference, as frequently used in ECoG studies (Ball et al., 2008, 2009b; Canolty et al., 2006, 2007). The simultaneously-recorded EEG was re-referenced to a separate CA reference. Similar to previous EEG studies (Dirlich et al., 1997), a peak detecting algorithm was used to determine the time point of the R-peaks from the ECG signal as a temporal reference for the following analysis. Since the pulse rate of the subjects never reached 2 Hz (120 heartbeats per minute) in the investigated time periods, the algorithm searched for peaks that were global maxima of the absolute ECG values in a time interval of 0.5 s before to 0.5 s after the detected peak. After the R-peak detection algorithm was applied, the ECG signal of each trial was visually inspected to avoid false-positive detected R-peaks due to contamination with artifacts. Data epochs were generated from −3 s to 3 s around each detected R-peak and each trial was baseline corrected using the median over time as a baseline. We then determined the average potential changes for each electrode as the median across trials. The median was used for better robustness against outliers.

Spectral analysis

For the time–frequency analysis, we used a multi-tapered spectral analysis method (Percival, 2000) with 3 Slepian tapers, a time window of 250 ms and 25-ms time steps. The spectral composition of the recorded signal was calculated separately for each electrode and trial. To compute the relative power changes for each electrode, we first determined the amplitude of the baseline for every individual frequency bin as the median over time and trials. Then we divided the time-resolved amplitude for each frequency bin by the frequency-specific baseline amplitude and calculated the median over trials for each time–frequency bin.

Phase synchrony

Phase-locking analysis can be used to investigate long-range neuronal integration from remote brain regions (Lachaux et al., 1999). If the phase difference between two separate but simultaneously-recorded event-related neuronal signals is consistent over trials, it is typically assumed that the corresponding brain regions are (directly or indirectly) functionally connected during the investigated event. To investigate heart cycle-related phase-locking characteristics, the phase of the signal was first computed for each time–frequency bin. To this end, complex-valued spectra were computed by Fourier transformation of the data in time windows of 250 ms moved in 25-ms time steps, for each electrode and trial. For each time–frequency bin, the phase difference between every possible ECoG electrode pair was calculated. Furthermore, the phase difference between every ECoG electrode and the ECG electrode was calculated in the

same way. For a specific electrode pair and a specific time–frequency bin, the phase synchrony value was determined in the following way: for each complex value of the Fourier-transformed data, the corresponding unit vector was calculated. After adding all unit vectors (one vector for each trial), the resulting complex value was divided by the number of trials. The norm of the result of this calculation is the phase synchrony index (which equals 1 if the phase difference is constant over all trials and is close to 0 in the case of random phase relations). The phase synchrony for each electrode pair was tested for significance against the null hypothesis of a random phase distribution by a two-sample Kolmogorov–Smirnov test. In the time–frequency window between 100 ms and 280 ms after the R-peak and from 1.5–12 Hz we determined ($p < 0.00001$; FDR-corrected (Benjamini et al., 2001) for the multiple tests over time–frequency bins) whether the observed phase distribution differed from a random distribution where all phase values have equal probability. This specific time–frequency window was chosen because the typical heart cycle-related spectral power increases in our data and in the previous literature were especially pronounced in this range (see Fig. 9c and Pérez et al., 2005).

Reduction of heart cycle-synchronized effects using template correction

Similar to template correction methods used in former EEG studies to minimize ECG artifacts (Barlow and Dubinsky, 1980), in a first step, we separately calculated the average potential as the median over trials for each ECoG channel to reduce heart cycle-synchronized effects. Then, for every channel the averaged potential was separately subtracted from every single heart cycle-related trial. After template correction, the same spectral analysis method and phase synchrony calculation was applied to the corrected trials and for the uncorrected trials.

Summary of latency data from previous HEP-related EEG studies

To compare our findings to those of previous studies in terms of evoked potential latencies, we systematically summarized the results of previous HEP-related EEG studies. Inclusion criteria were as follows: Studies had to report on HEPs in EEG recordings. Time information on the HEPs had to be provided relative to the ECG R-peak. Studies that met these requirements included HEP-related EEG studies with uninformed participants (Dirlich et al., 1998; Pérez et al., 2005), studies investigating the modulation of HEPs due to psychological factors like attention, motivation or the ability to consciously perceive heartbeats (Montoya et al., 1993; Pollatos and Schandry, 2004; Pollatos et al., 2005; Schandry and Weitkunat, 1990; Schandry et al., 1986; Yuan et al., 2007), and studies investigating the modulation of HEPs in the context of pain perception (Shao et al., 2011), empathy (Fukushima et al., 2011), diabetic neuropathy (Leopold and Schandry, 2001) and stress (Gray et al., 2007). Overall, 12 EEG studies (Table 2) were included. The number of studies reporting HEP occurrence or modulation was determined in a time-resolved way as shown color coded in Fig. 6c.

Results

Ongoing ECoG recordings and R-peak triggered averaged ECoG data

Ten seconds of raw data from simultaneously-recorded ECG and ECoG signals of P1 is shown in Fig. 2. The inter-hemispherical implanted strip electrode IHC-4 (Fig. 2; 5th trace) recorded persistent oscillatory potential changes whose frequency matched the pulse rate. Small amplitude heart cycle-related potentials in recordings from other subdurally-implanted electrodes, if present, may have been masked by ongoing high amplitude activity.

To investigate the temporal properties of the recorded signals, we performed heart cycle-related trial averaging with a large number of trials, similar to previous studies with scalp EEG recordings (Dirlich et al., 1997, 1998). Resulting trial-averaged potentials from the same electrode contacts as in Fig. 2 are shown in Fig. 3. As expected, the average potentials recorded from the inter-hemispherically-implanted strip electrode IHC-4 (Fig. 3b) showed a clear oscillation similar to the ongoing recordings in Fig. 2. Comparable heart cycle-related potentials with lower amplitude also became evident in the recordings of grid electrode G-F3 (Fig. 3c), even though in this example, there were no pronounced heart cycle-related potentials in the ongoing recordings (Fig. 2). The frontally-located electrode G-B1 (Fig. 3e) recorded heart cycle-related potential changes with a steep rising edge and a flat slope, while the nearby electrode G-B3 (Fig. 3d) recorded no pronounced potential changes. Grid electrode G-D7 (Fig. 3f) located on the somatosensory cortex recorded a delayed biphasic potential starting approx. 200 ms after the R-peak.

Characterization of heart cycle-related potential changes in ECoG

For the following characterization of the invasively-recorded heart cycle-related potential changes, we refer to the results of earlier non-invasive EEG studies. As summarized in the Introduction section, three distinct effects have been reported in the previous EEG literature: the HEP, the CFA and the pulsatility artifacts (Table 1). We anticipated that these three types of heart cycle-related potential changes would occur in ECoG recordings, too. Indeed, in the heart cycle-related averaged ECoG data, we found effects with the hypothesized spatial and temporal characteristics as follow:

I) Late biphasic potentials

A late biphasic potential (highlighted with gray circles in Fig. 4) similar to the potential recorded from the electrode G-D7 (Fig. 3f)

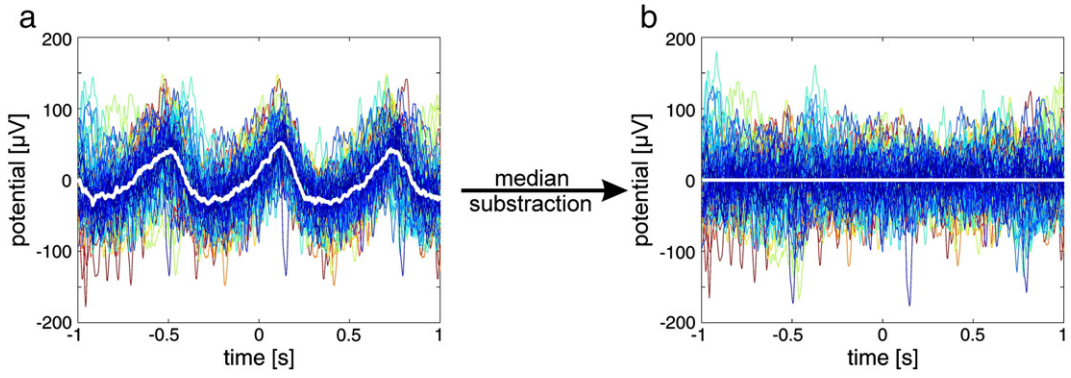

Fig. 1. Template correction a) Exemplary oscillatory potentials (median in white and 100 individual trials in color) recorded with strip electrode IHC-4 of P1. b) Corrected heart cycle-related potentials after subtracting the median potential from every single trial. Colored lines: individual trials; white line: median over trials. The oscillatory pattern of the averaged heart cycle-related potentials recorded with strip electrode IHC-4 expectedly disappeared after artifact correction.

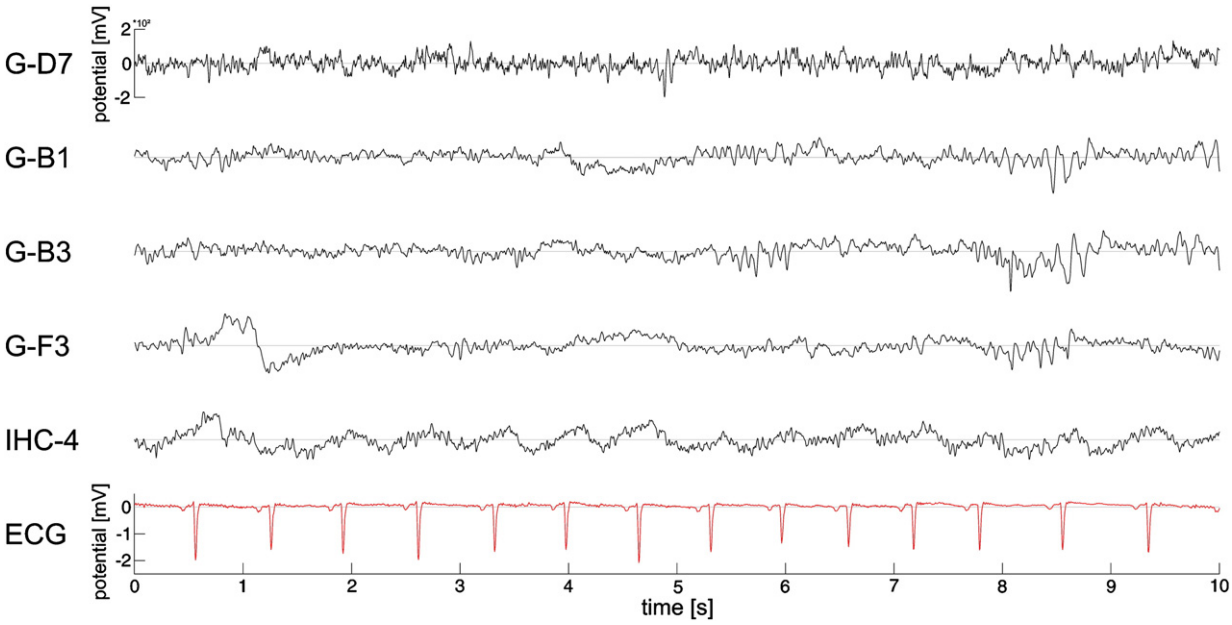

Fig. 2. Ongoing ECoG/ECG recordings (P1); example of ongoing recordings from subdurally-implanted grid electrodes (electrode labels starting with G-) and from one inter-hemispherically-implanted strip electrode (IHC-4) is shown. No clear heart cycle-related potential changes were evident in the ECoG traces of the grid electrodes, but recordings from the strip electrode IHC-4 showed clear persistent oscillatory potential changes with a frequency matching the pulse rate. Amplitude scale of the topmost trace applies to all ECoG traces.

in P1 was also recorded in adjacent electrode contacts located on or near the left somatosensory cortex. Similar biphasic potentials were also observed over the left and right somatosensory cortices of P2 and P3, respectively (Figs. S1, S2). A superimposed plot of these potentials illustrates their similarity (Fig. 6b). The grand average over all potentials showed a positive peak at ~280 ms and a negative peak at ~360 ms (Fig. 6c). As illustrated on a standard brain surface (Fig. 6a), the biphasic potentials were found in a circumscribed area within the somatosensory cortex (note that this area was not covered by the electrode-grid in P4, P5 and P6).

II) Sharp ECoG potentials at the time of the ECG R-peak

A sharp potential at the time of the ECG R-peak is typical for the time course of the CFA in EEG recordings. Such a potential was not evident in any ECoG recordings except those of P4 (Fig. 5; highlighted

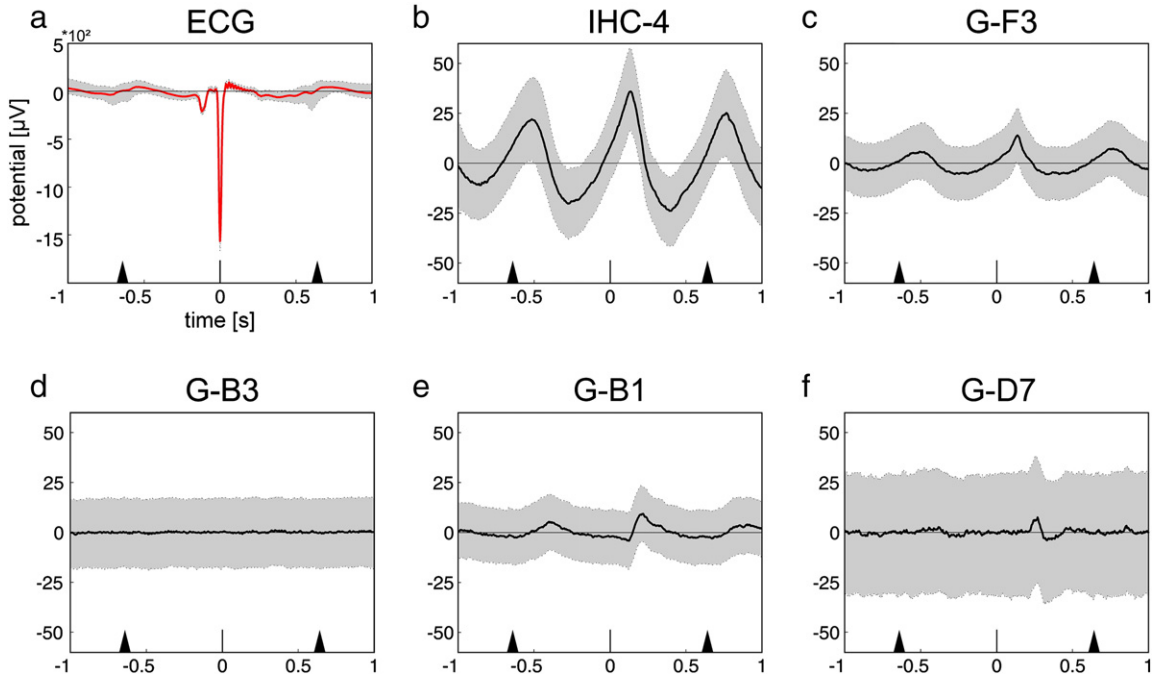

Fig. 3. Trial-averaged potential changes in ECoG/ECG recordings (P1) relative to the ECG R peak. At the bottom of each panel, the median time points of the preceding and subsequent R-peaks are depicted by the tip of the black triangles. The pulse variability (25th to 75th percentile) is indicated by the length of the triangle's base. Red curve (a) and black curves (b–f) represent the average heart cycle-related potential as the median over trials (2270 trials); gray bands extend from the 25th to the 75th percentile of the data; a) ECG potential changes b) potential changes recorded with the inter-hemispherically-implanted strip electrode IHC-4 c–f) potential changes recorded with grid electrodes G-F3, G-B3 and G-B1 located over the left frontal cortex and G-D7 located over the left primary somatosensory cortex of P1 (see fig. 4).

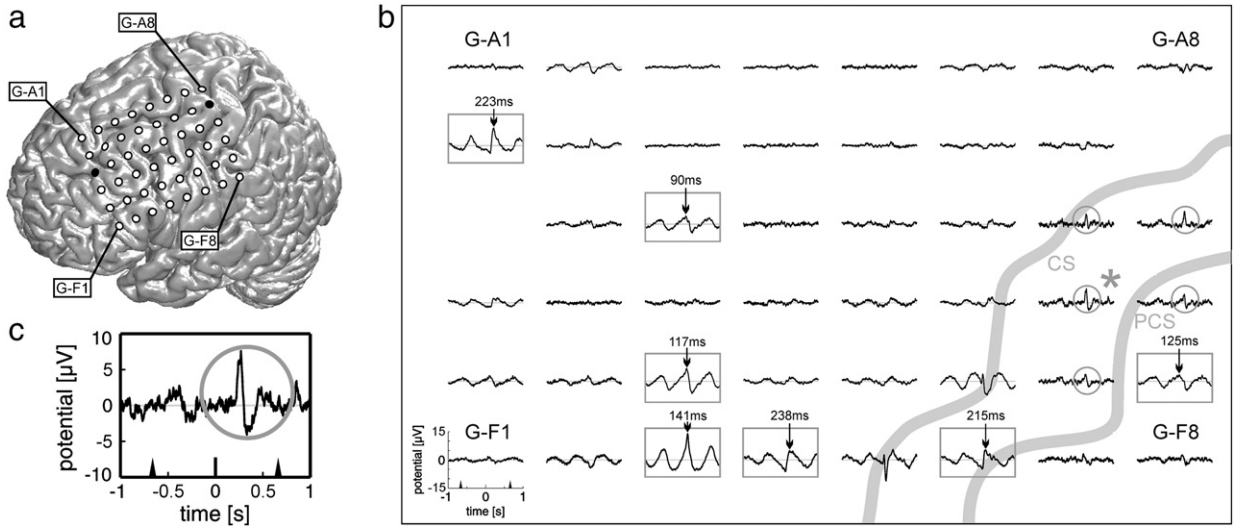

Fig. 4. Heart cycle-related ECoG potential changes: oscillatory potential changes matching the heart pulse rate and late biphasic potentials (P1). a) Location of the electrode-grid of P1 superimposed on a standard brain surface. Circles represent the electrode contacts as determined from a structural MRI scan. Black circles represent electrode contacts that were dropped from the analysis due to poor contact to the cortical surface. b) Averaged potentials for each electrode contact; the scale in the lower left corner of the plot applies to all ECoG traces in the figure. The course of the central sulcus (CS) and the post-central sulcus (PCS) in relation to the electrode positions is depicted by gray lines. High amplitude oscillatory potential changes (examples highlighted by gray rectangles) were widely distributed and had different peak latencies (represented by arrowheads). Biphasic potential changes (highlighted by gray circles) were recorded between CS and PCS (G-C7, G-C8, G-D7 and G-E7) and nearby (G-D8). c) Magnification of the biphasic potential changes in ECoG electrode contact G-D7 (marked with gray asterisk in (b)).

by gray triangles). Even in this case, the low-amplitude peaks were barely observable, in contrast to the high-amplitude oscillatory potential changes. Some electrodes at the posterior-medial edge of the electrode-grid recorded sharp peaks with positive amplitude (Fig. 5; gray triangles with the tip up), others at the anterior-lateral edge of the electrode-grid recorded sharp peaks with negative amplitude (Fig. 5; inverted gray triangles) at time point zero.

III) Oscillatory potential changes matching the heart pulse rate

Heart cycle-related oscillatory potential changes matching the heart pulse rate similar to the examples from P1 (Figs. 3b, c, e) were observed in all patients investigated. The shape of these waves was typically smooth wave- (e.g., Figs. 3b, c) or saw-tooth-like (e.g., Fig. 3e). Hence, the time courses of the invasively-recorded oscillatory potential changes matched the known pulsatility artifacts in non-invasive EEG recordings. In contrast to the relatively invariable delay of ~200 ms (relative to the ECG R-peak) typical for the pulsatility artifact peaks in non-invasive EEG (Hirsch and Brenner, 2010; Zumsteg et al., 2004), the peaks of the invasively-recorded oscillatory potential changes differed considerably both between and within patients (Figs. 4, 5, S1 and S2).

Heart cycle-related effects in simultaneously-recorded EEG and ECoG

Next, we compared heart cycle-related potential changes in the ECoG and in the simultaneously-recorded non-invasive EEG. Given that the findings were very similar for all patients, only examples from patient 4 are shown (Fig. 7). The dominant feature of heart

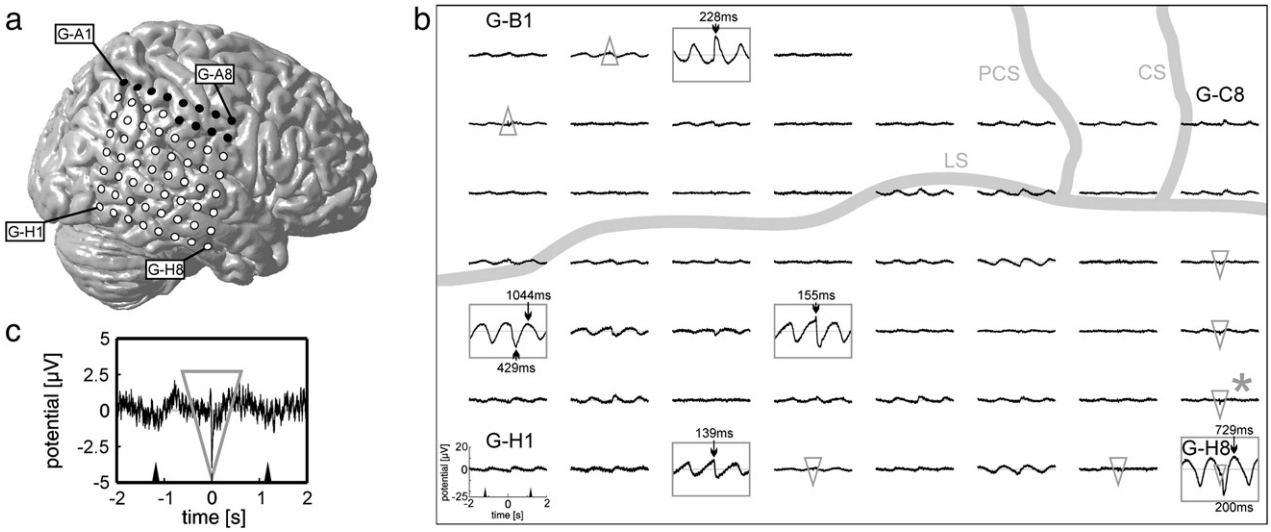

Fig. 5. Heart cycle-related ECoG potential changes: oscillatory potential changes matching the heart pulse rate and sharp peaks (P4). As in P1 (Fig. 4), high amplitude oscillatory potential changes were widely distributed (highlighted by gray rectangles). A few electrodes were contaminated with the CFA, either with a positive peak at time point zero (highlighted by gray triangles) or with a negative peak (highlighted by inverted gray triangles). c) Magnification of the CFA of ECoG electrode contact G-G8 (marked with gray asterisk in (b)); all conventions as in Fig. 4; black circles represent defective electrode contacts.

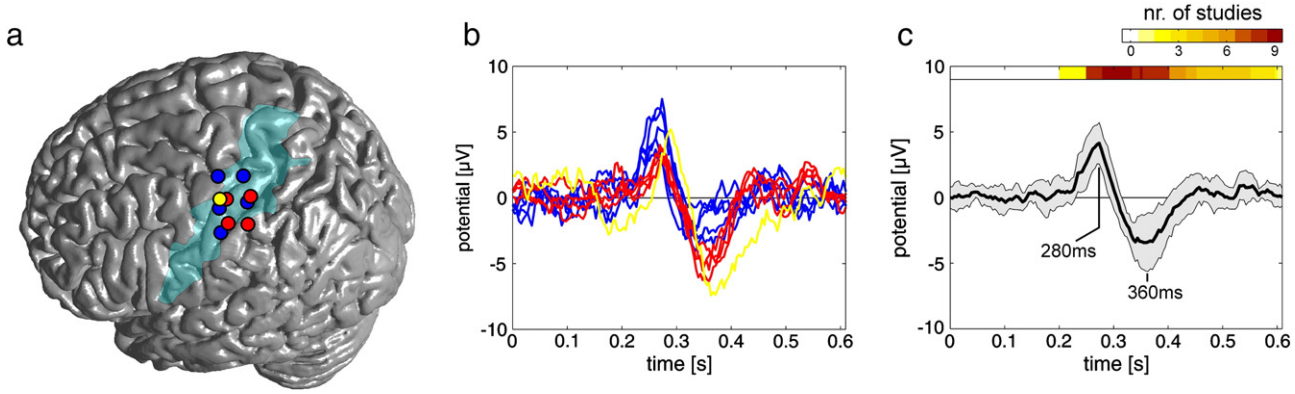

Fig. 6. The delayed biphasic heart cycle-related potential. On the left side (a), electrode contacts that recorded the biphasic potential (represented as colored circles) are shown superimposed on a standard brain surface; blue, red and yellow circles correspond to electrode contacts of P1, P2, and P3, respectively (in P3, the electrode position was mirrored to the left hemisphere for better inter-individual comparison); the transparent blue area indicates the left somatosensory cortex, as determined from the probabilistic maps from the Anatomy Toolbox 1.6 in SPM5. b) Time course of all biphasic potentials at the electrode contacts shown in (a); color coded as in (a); c) Grand average over all selected electrodes; the black curve represents the average potential as the mean over electrodes; the corresponding standard deviation is coded as gray band. The HEP latency of all 12 EEG studies from Table 2 is shown at the top of the graph. The absolute number of studies reporting HEP occurrence at the corresponding point in time is color coded. The latency of the biphasic heart cycle-related potential is in good accordance with the existing literature about HEP latency in EEG recordings.

cycle-dependent potential changes in EEG recordings was the CFA. Originating from myocardial muscle activity, the CFA manifested itself by a sharp peak at time point zero (Fig. 7a), corresponding to the ECG R-peak. The shape of this sharp peak (e.g., EEG electrode T2 in Fig. 7b) was nearly indistinguishable from the time-course of the ECG during the QRST segment of the cardiac cycle (Fig. 3a). A polarity reversal was observed at the midline, as expected due to the CA referencing. The amplitude of CFA peaks in the EEG recordings reached absolute values up to 17 μV (Fig. 7b), while the corresponding amplitude of sharp peaks in simultaneously-recorded ECoG was below 4 μV

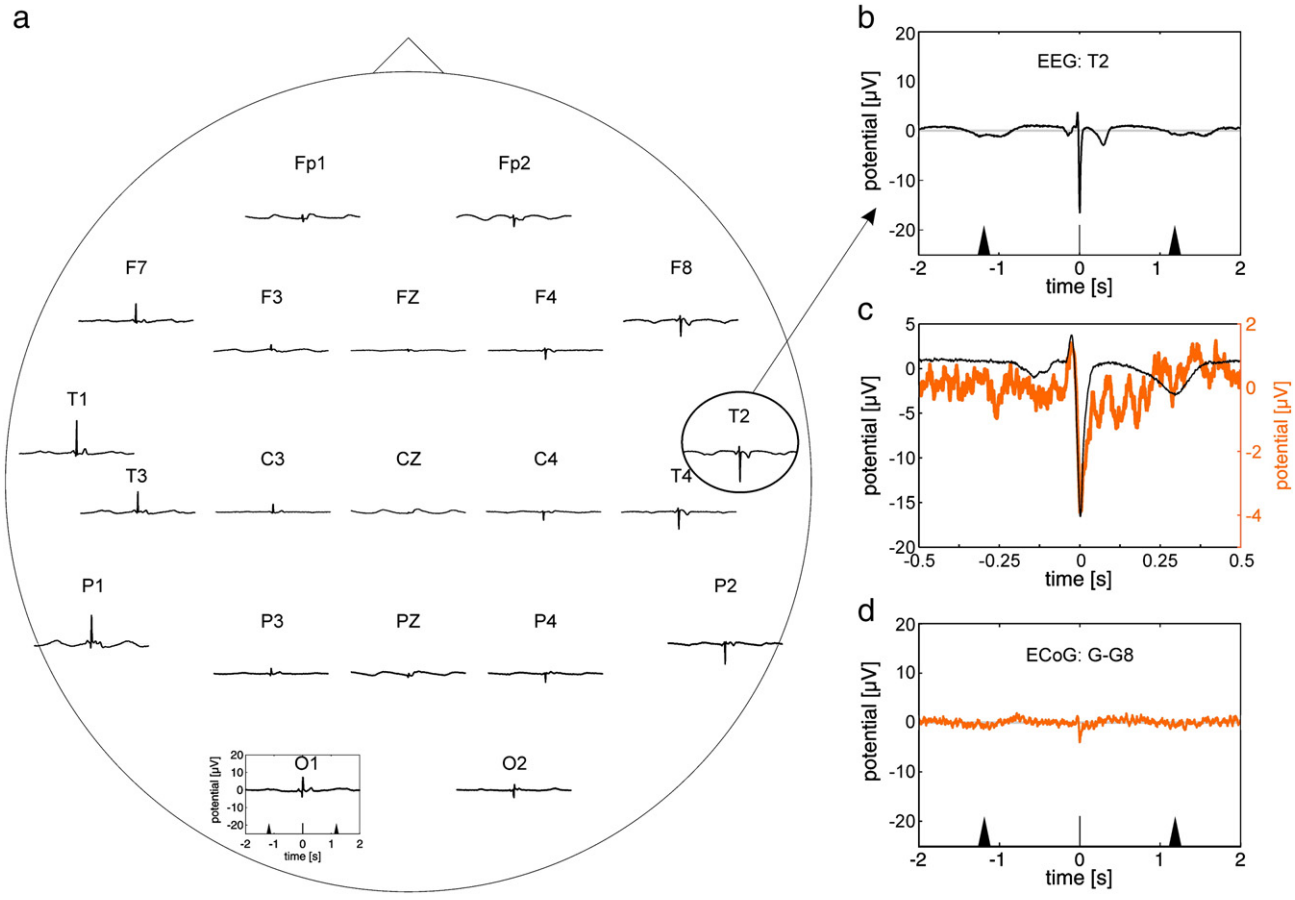

Fig. 7. Heart cycle-related non-invasive EEG potential changes (P4). The averaged potential for each EEG electrode contact is shown in (a); the scale of the electrode O1 in the lower left of the plot applies to all electrode contacts in (a). The timing of the preceding and subsequent R-peaks is illustrated as in Fig. 4; b) magnification of the potential recorded at EEG electrode contact T2; c) black curve represents scale-up of the potential changes recorded with EEG electrode contact T2; orange curve represents the superimposed time course of the simultaneously-recorded ECoG potentials at grid electrode G-G8; d) median potential recorded at ECoG grid electrode contact G-G8; The time course of the potential recorded with grid electrode G-G8 is very similar to the time course of the potential recorded with EEG electrode contact T2 during the QR segment of the cardiac cycle.

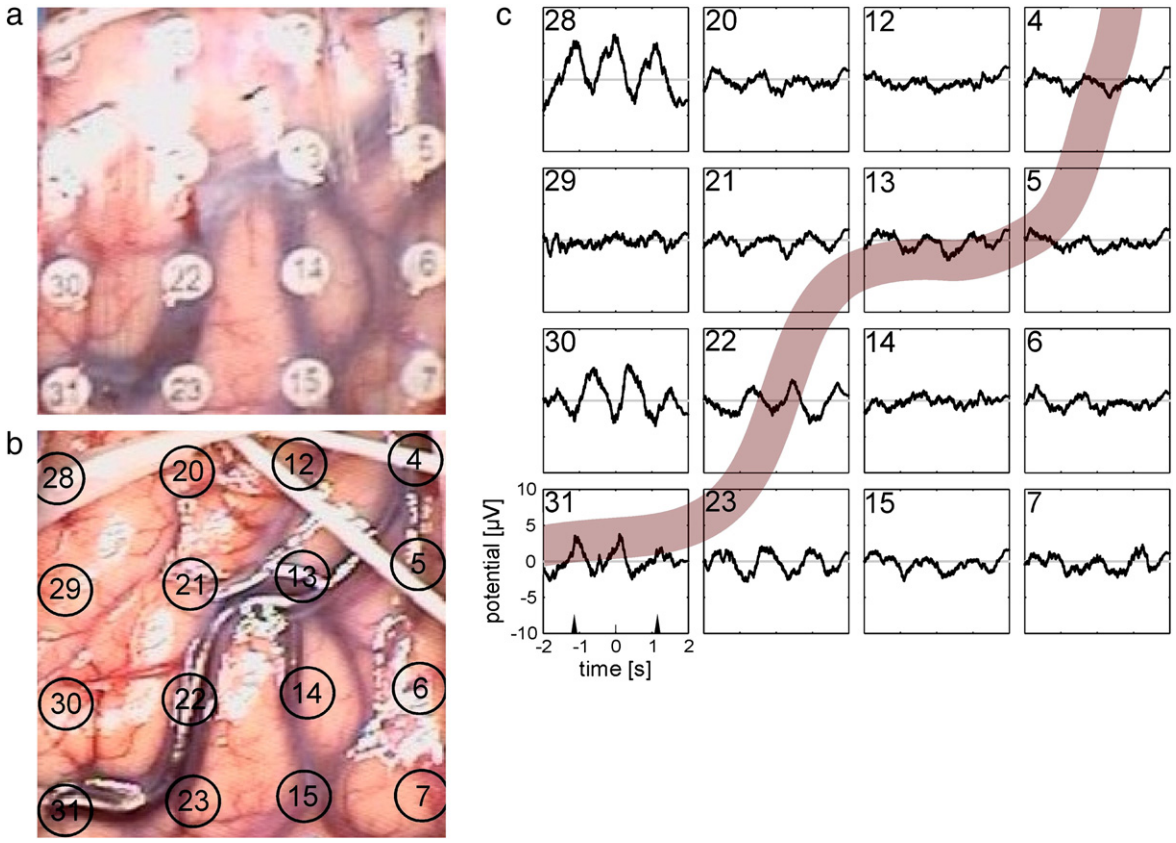

Fig. 8. Intra-operatively-acquired photograph. View of the cortical surface after (a) and before electrode placement (b) in P5. In (b), black circles indicate the location of the electrode contacts on the brain surface and relative to the subdural blood vessels. c) Average potential as a median for each electrode contact. The dark red line marks the course of the vena anastomotica inferior (Labbé). Slow oscillatory potential changes were recorded independently of electrode position in relation to the Labbé.

(Fig. 7d). Thus, the CFA peaks in EEG were approximately four times higher in amplitude than the sharp peaks in ECoG (Fig. 7c) that we assume to be ECoG manifestations of the CFA (see Discussion section).

Another distinct feature in the EEG recordings of this study was an oscillatory pattern, consisting of smooth waves synchronous to the heart pulse of the subject. This feature was observed in all investigated

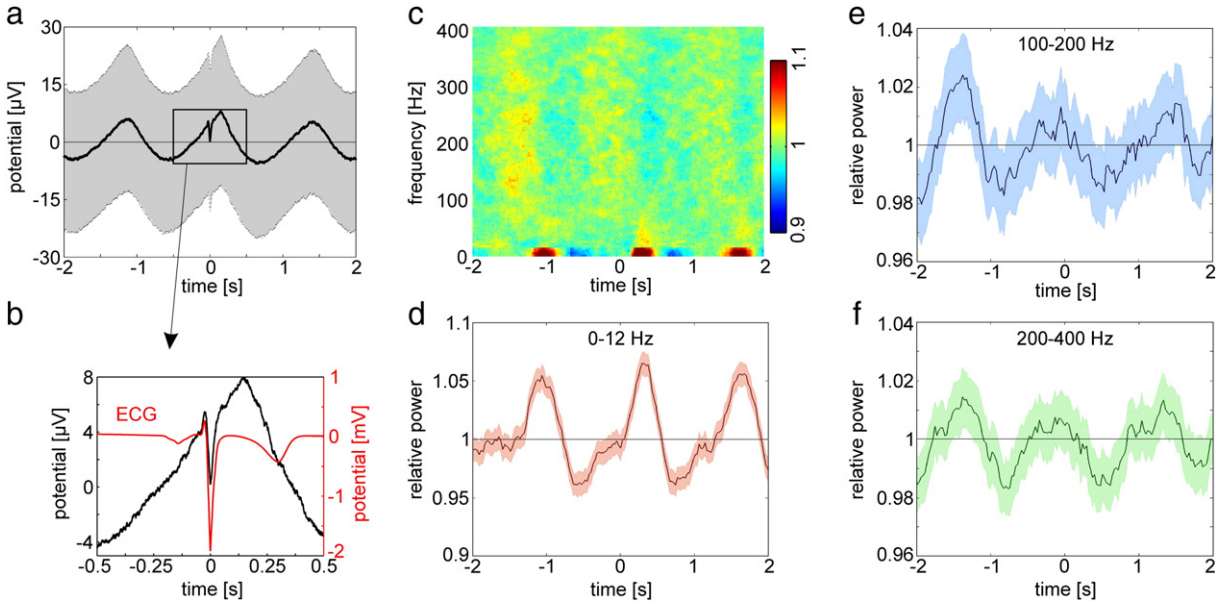

Fig. 9. Spectral composition of an exemplary oscillatory potential matching the heart pulse rate (P4). a) R-peak triggered potential recorded with electrode contact TBA-4 of P4; black curves represent the averaged pulse-related potential as the median over trials; gray bands extend from the 25th to the 75th percentile of the data; b) black curve represents scale-up of the CFA recorded with electrode contact TBA-4; red curve represents the superimposed time course of the simultaneously-recorded ECG channel; c) spectral composition of the signal with relative power, color coded from 0.9 to 1.1; d–f) corresponding frequency-band-power changes for (d) very low (0–12 Hz), (e) high (100–200) and (f) very high (200–400 Hz) frequency bands; colored bands extend from the 25th to the 75th percentile of the data. In summary, the electrode contact TBA-4 recorded pronounced potential changes (oscillatory potential changes matching the pulse rate and a sharp peak at 0 s) as well as pronounced spectral power changes.

subjects; an example of EEG recordings from patient 4 is shown in Fig. 7a. The smooth-wave pattern was superimposed by the CFA during the QRST segment of the cardiac cycle in most cases (Figs. 7a; e.g., Fp1, FP2 and P1). In comparison to the pulsatility artifacts in EEG, the oscillatory pattern in ECoG that we assume to be manifestations of pulsatility artifacts (see Discussion section) were approx. six times larger in amplitude. Clear examples of an HEP, as observed with ECoG over the somatosensory cortex, were not noticeable in any of the simultaneously-recorded EEG channels.

Effects of cortical blood vessels on heart cycle-related effects in ECoG

Intra-operatively-acquired photographs before and after electrode placement over the left temporal cortex (Fig. 8) were used to determine the spatial relation of electrodes with pulsatility artifacts and subdural blood vessels. In P5, electrode contacts 13, 22 and 31 (Fig. 8) located on the vena anastomotica inferior (Labbé) recorded slow oscillatory potentials, synchronous to the heart pulse of the patient, but electrode contact 30 (Fig. 8) clearly located next to the Labbé vein also did so, in almost the same manner. Electrode contact 14 (Fig. 8) located on a branch of the Labbé vein and electrode contact 29 (Fig. 8) located adjacent to the Labbé vein recorded only marginal potential changes. Similar results were also observed in the prefrontal region recorded in P6

Spectral power changes

Oscillatory potential changes matching the pulse rate were recorded, for example, with the temporo-basally-implanted strip electrode contact TBA-4 (Fig. 9a). In this channel, also a pronounced sharp peak at 0 ms with negative amplitude was recorded, the time course of which was comparable to the ECG during the QR segment of the cardiac cycle (Fig. 9b; −30 ms to 0 ms). The spectral composition of the recorded signal is shown in Fig. 9c. Spectral power changes were not only most prominent in the very low-frequency range (Fig. 9d; 0–12 Hz), but also noticeable in the high- (Fig. 9e; 100–200 Hz) and very high- (Fig. 9f; 200–400 Hz) frequency ranges.

Heart cycle-related spectral power changes for all grid electrodes of P4 are shown in Fig. 10. The spectral power changes from four electrodes that showed oscillatory potential changes with the highest peak-to-peak amplitude (Fig. 10b; highlighted by black rectangles) are magnified on the right (Fig. 10d). Regarding the spectral power changes recorded with these electrode contacts, the most prominent modulations were in the low-frequency range, but still noticeable in the high- and very high-frequency ranges, similar to the recordings of the electrode contact TBA-4 (Fig. 9).

Results of template correction

Oscillatory potentials synchronous to the heartbeat were the dominant feature in the presented heart cycle-related ECoG recordings (Figs. 4, 5, S1 and S2; gray rectangles). To reduce these probably artificial oscillatory potentials in our ECoG recordings, we performed a template correction by subtracting the average heart cycle-related potential from every single trial (as described in the Materials and methods section). Exemplary oscillatory potential changes were observed in the recordings from the inter-hemispherical implanted strip electrode IHC-4 of P1 (Fig. 3b). We used 100 trials of R-peak triggered ECoG recordings from that electrode channel to illustrate the template correction method (Fig. 1). In the uncorrected recordings of strip electrode IHC-4, the oscillatory pattern was even observable in single trials (Fig. 1a; colored lines) and clear-cut in the averaged median potential (Fig. 1a; white line). After subtracting the median potential, the oscillatory pattern of the heart cycle-related recordings was less evident in the potential range of single trials (Fig. 1b; colored lines) and expectedly disappeared completely in the corrected averaged potential (Fig. 1b; white line).

Heart cycle-related phase synchrony

High phase synchrony indices (PSIs) between ECoG channels and the ECG were observed in the low frequency range from 1.5 Hz to 12 Hz. These effects occurred in the time window between 100 ms and 280 ms after the R-peak in all patients investigated. Additionally, ECoG channels with strong phase synchrony with the ECG tended to strong phase synchrony between each other in this specific time–frequency range (Fig. 11a). For example, the inter-hemispherically-implanted strip electrode IHC-4 recorded signals with strong phase synchrony to the ECG (Fig. 11a; white circle 1), just like the grid electrode F3 (Fig. 11a; white circle 2). Resultant phase synchrony was observed between these ECoG channels (Fig. 11a; white circle 4).

After subtracting the average potential changes from every trial of each channel separately, as described in the Materials and methods section, the high phase synchrony between ECoG channels and the ECG decreased considerably (Fig. 11b). Furthermore, the strong phase synchrony between these ECoG channels (e.g., F3 to IHC4; Fig. 11b) decreased as well. ECoG channels with low PSI to the ECG, but high PSI between each other were not affected by the template correction (Fig. 11b; e.g., white circles 6–7). Some of the highest PSIs before as well as after template correction were observed between nearby ECoG channels (Fig. 11b; e.g., white circles 8 and 9). As shown in Fig. 11c, many PSIs between ECoG channels decreased considerably due to the template correction (below the diagonal), some PSIs remained relatively unchanged (on/close to the diagonal), and in some cases the PSI increased slightly (slightly above the diagonal).

Discussion

In this study, we investigated heart cycle-related effects on simultaneously-recorded EEG and ECoG. In the ECoG recordings, we identified all three types of heart cycle-related effects previously described in non-invasive EEG: HEPs, CFAs and pulsatility artifacts. These three types of effects matched well to our expectations based on literature on the non-invasive EEG (Table 1).

Somatosensory components of the HEP in the ECoG

Heartbeat-evoked potentials (HEPs) and their modulation due to psychological factors in EEG have been frequently investigated in the context of heartbeat perception. Possible neuronal sources of the reported HEPs included somatosensory cortex, frontal regions (Dirlich et al., 1998; Leopold and Schandry, 2001; Montoya et al., 1993; Pollatos and Schandry, 2004; Schandry and Weitkunat, 1990; Schandry et al., 1986) as well as cingulate and insular cortices (Cameron and Minoshima, 2002; Critchley et al., 2004; Khalsa et al., 2009; Pollatos et al., 2005). In the present study, potential changes with a delayed biphasic pattern were consistently recorded on ECoG electrodes located over a region within the somatosensory cortex (Fig. 6a). These delayed biphasic signals had a similar time course across patients and electrode contacts (Fig. 6b), and had a positive peak at ~280 ms and a negative peak at ~360 ms (Fig. 6c). The reported latencies of HEPs in EEG are not completely consistent across published studies and vary between 200 ms and 650 ms after the R-peak (Table 2). The most frequently reported HEP latencies are in the time interval from 255 ms to 400 ms (8 of the 12 selected HEP-related EEG studies). Schandry and Weitkunat, (1990) estimated an expected HEP latency assuming a pressure peak in the left ventricle of the heart and the aorta 180 ms and 220 ms post-R-wave, respectively, and taking into account the latency of brain responses after urinary bladder nerve stimulation (between 100 ms and

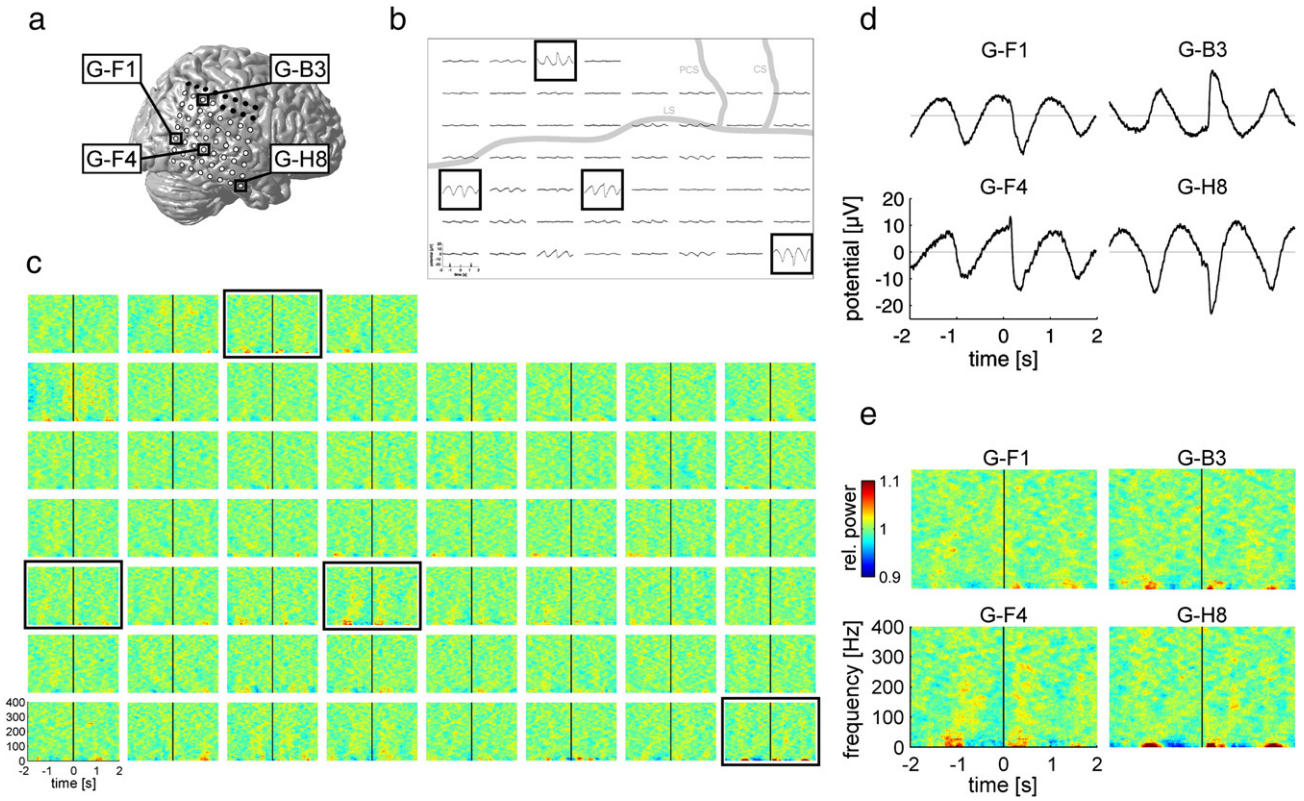

Fig. 10. Topography of heart cycle-related spectral power changes (P4). a) Location of the electrode-grid superimposed on the brain surface of the implanted patient; b) averaged heart cycle-related potentials (same as in Fig. 5). c) Relative spectral power changes for all active grid electrodes in the same time range as in (b) and color coded from 0.9 to 1.1. Black squares indicate the location of electrode contacts that recorded the slow oscillatory potential changes with high peak-to-peak amplitude. Averaged potentials (d) and corresponding relative spectral power changes (e) recorded with the selected grid electrodes G-F1, G-B3, G-F4 and G-H8 are shown in detail. Pronounced spectral power changes even in the high frequency domain accompanied the slow oscillatory potential changes.

150 ms). They concluded that the HEP latency should be in the range of 280 ms to 370 ms relative to the ECG R-peak. These values fit very well with the latencies of the biphasic ECoG responses that we find over the somatosensory cortex (280 ms to 360 ms).

Thus, we conclude that it is very likely that these delayed biphasic responses represent brain activity related to the processing of cardiac-related information via a somatosensory pathway. These findings would confirm the assumption that somatosensory cortex, a frequently-discussed source of HEPs in former EEG studies (Dirlich et al., 1998; Leopold and Schandry, 2001; Montoya et al., 1993; Pollatos and Schandry, 2004; Schandry and Weitkunat, 1990; Schandry et al., 1986) indeed plays a role in the processing of cardiac information.

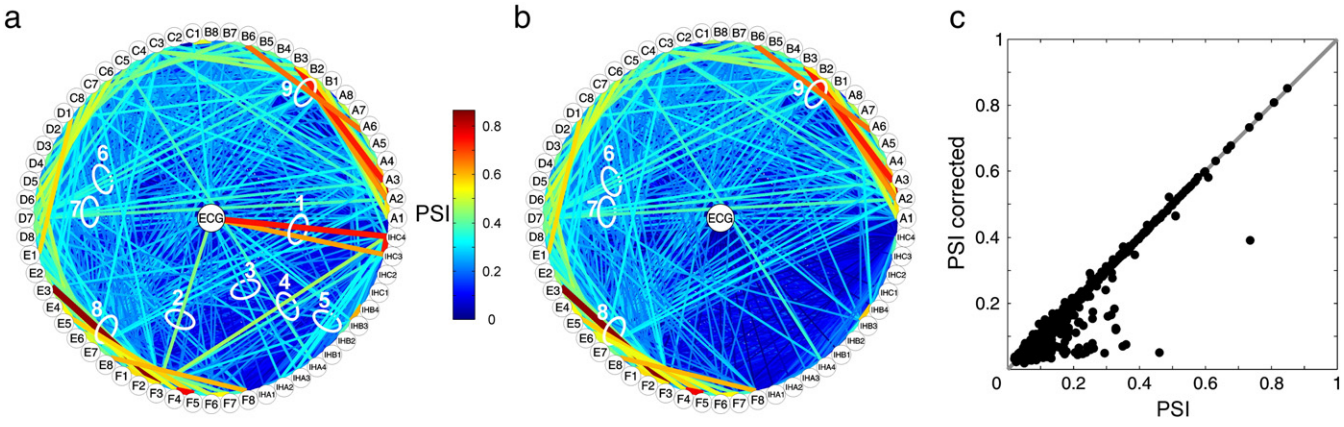

Fig. 11. Heart cycle-related phase synchrony in the very low frequency range (1.5 to 12 Hz) in P1. a) Phase synchrony in the very low frequency range (1.5 to 12 Hz) in a time window of 100 ms to 280 ms after the ECG R-peak between recordings from ECoG electrodes (on the circular line) and an electrode recording the ECG signal (in the center of the circle). Value of phase synchrony between electrode pairs is coded with phase-synchrony-index (PSI)-dependent colors of the connecting lines between the correspondent electrodes. Higher PSIs are also highlighted by the use of thicker lines. White circles 1–3 highlight the highest PSIs of ECoG channels to the ECG channel, while the circles 4–5 bundle the PSIs between these ECoG channels. 6 and 7 illustrate high PSIs between distant ECoG channels that were not phase-locked to the ECG channel. 8 and 9 highlight high PSIs of nearby ECoG channels; b) PSIs between electrode pairs as in a), but after subtracting the average potential (as the median over trials) from every single trial separately for each electrode. Note that the high PSIs between ECoG electrodes and the ECG channel (white circles 1–3 in a), as well as the high PSIs between these ECoG electrodes (white circles 4–5 in a) decreased. High PSIs between ECG-independent-ECoG electrodes (white circles 6–9) were not affected; c) Overview of all PSIs between ECoG channels; every black dot represents one electrode pair, with x-value corresponding to the original PSIs and the y-value corresponding to the PSIs after the ECG correction.

CFAs in the ECoG

The CFA in scalp EEG recordings was previously described to be most prominent during the QRS complex of the heart cycle and to a lesser extent during the T wave (Dirlich et al., 1997). As the observed potential changes in the ECoG signals match the CFA in the EEG in terms of time course and polarity characteristics, it seems unlikely that these potential changes in the ECoG recordings represent responses of heart cycle-related brain activity. Rather, they appear to be an intracranial manifestation of the CFA. But, in contrast to the CFA in EEG recordings, the potential changes in ECoG recordings were less consistent across patients and electrode contacts and smaller in amplitude.

Pulsatility artifacts in ECoG

Oscillatory potential changes matching the pulse rate were a surprisingly prominent feature of many ECoG channels in all patients investigated in the present study (Figs. 3, 4, S1 and S2). The observed smooth wave- and saw-tooth-like time course of these oscillatory potential changes matched the shape of pulsatility artifacts reported in EEG (Binnie, 2003; Cooper et al., 2003a; Dworetzky et al., 2010; Hirsch and Brenner, 2010; Stern, 2004; Zumsteg et al., 2004). Such artifacts are thought to result from impedance changes caused by electrode displacement (Misra, 2005). Our comparison of the position of subdural blood vessels and the sites of oscillatory ECoG changes based on intra-operatively-acquired photographs before and after electrode placement (Fig. 8) did not support the hypothesis that slow oscillatory potentials were solely recorded from electrode contacts directly located on large blood vessels. Epidural vessels, pulsatile CSF circulation and cardiac cycle-dependent brain motion could have contributed to the observed effects in electrodes that were not located on large subdural vessels and still recorded wavelike potential changes.

Comparison of heart cycle-related effects in EEG and ECoG

Because they are located at close range to the brain surface, implanted ECoG electrodes allow recording brain signals with considerably higher amplitude and spatial resolution than recordings with EEG scalp electrodes (Engel et al., 2005). Additionally, ECoG recordings were repeatedly emphasized to be less susceptible to muscle artifact contamination (Ball et al., 2004; Canolty et al., 2007; Engel et al., 2005; Lachaux et al., 2003; Leuthardt et al., 2004; Schalk et al., 2007). In a recently published study, we reported that under certain circumstances blink- and eye movement-related artifacts can affect ECoG studies, in particular in the prefrontal and anterior temporal areas (Ball et al., 2009a; Jerbi et al., 2009). Amplitudes of blink-related artifacts in ECoG ranged from approx. 10 μV to approx. 23 μV, thus being of similar size as (small) event-related potentials reported in the ECoG literature. By using the amplitudes of eye-blink artifacts and ongoing brain activity as a reference, we calculated that the SNR of invasive ECoG is however 20 to 100 times better than that of simultaneously-recorded non-invasive EEG.

In the present study, we found the maximal amplitude of the CFAs to be approx. 4 μV, hence smaller than in the simultaneously-recorded non-invasive EEG (~17 μV) and also considerably smaller than the above-mentioned amplitudes of blink-related artifacts in ECoG recordings. It should also be taken into account that, in contrast to the EEG where CFA contamination was the dominant feature in recordings of all patients, CFA contamination in the ECoG recordings of four (P1, P2, P3 and P5) out of five patients included in this study was not noticeable at all. Thus, it seems that blood vessels acting as low conductance pathways through which the CFA "tunnels" into the intracranial cavity is not a common phenomenon. Otherwise, CFA contamination in ECoG recordings should have been more consistent over patients. We can definitely affirm that veins do not necessarily act as low conductance pathways, since recordings of electrode contacts located directly on the vena anastomotica inferior (Labbé) of P5 were not noticeably contaminated with the CFA. A "reverse breach rhythm", causing myocardial EMG to penetrate to the intracranial space through the inter-individually variable bone defects due to craniotomy carried out for electrode implantation (personal communication from Dr. Jean Gotman reported in Otsubo et al., 2008) could be responsible for the inter-individual differences with respect to CFA contamination. Differences between EEG and ECoG with regard to CFA amplitude also may depend on the re-referencing method. The CFA may become better visible/more problematic with other re-referencing than the CA reference used throughout the study, particularly in the ECoG data. In comparison to the amplitude of the CFA in EEG recordings and by taking into account that brain signals in ECoG recordings are of considerably higher amplitude than in EEG, we conclude that CFA contamination in ECoG is by far less a problem for the investigation of heart cycle related neuronal signals than it is in EEG.

The maximal amplitudes of pulsatility artifacts in ECoG recordings in the present study ranged from 15 μV to 28 μV, whereas corresponding artifacts in EEG recordings were only around 5 μV in amplitude. This is to our knowledge the first example of artifacts that are of higher amplitude in ECoG recordings than in simultaneously-recorded EEG. These pulsatility artifacts in ECoG are of similar amplitude as eye-blink artifacts and hence of similar size as (small) event-related potentials reported in the ECoG literature (Ball et al., 2009a). All three proposed origins of pulsatility artifacts in EEG, i.e., pulsating blood vessels, pulsatile circulation of CSF and the resulting pulsatile motion of brain tissue, can all also be considered as possible sources of the pronounced pulsatility artifacts in ECoG. In scalp EEG, it is common practice to change the location of individually-placed electrodes if they show strong pulsatility artifacts in ongoing recordings, while this is not possible in ECoG. This difference in combination with the proximity of the implanted electrode contacts to blood vessels, pulsatile circulation of CSF and pulsatile motion of brain tissue may have contributed to the higher amplitudes of pulsatility artifacts in ECoG compared to EEG. The pronounced pulsatility artifacts in the ECoG grids may also depend on postoperative swelling and the build-up of intracranial pressure. Regarding the topic of HEPs in our non-invasive EEG data, see Supplementary discussion.

In summary, ECoG recordings are more susceptible to pulsatility artifacts than scalp EEG, given that maximal amplitudes of pulsatility artifacts were approx. six times larger in ECoG than in the simultaneously recorded EEG. By contrast, the situation is the other way around with regard to the CFA: its maximal amplitude was approx. four times larger in the EEG than in the ECoG. CFA contamination was the dominant feature in almost every EEG channel in all patients investigated, while ECoG channels were hardly ever affected. Given that the spatial resolution of ECoG is much better than that of scalp EEG and artifact contamination (both CFAs and pulsatility artifacts) was limited to only a subset of ECoG electrodes, the ECoG appears to be much better-suited for investigating HEPs than the non-invasive EEG. In fact, the present study is, to our knowledge, the first to show an HEP with a stereotypical time course and topographical distribution both clearly and consistently observed across subjects.

Heart cycle-related changes in spectral power and inter-channel phase synchrony

In addition to our investigation of the time-domain signal, we used time–frequency analysis to investigate the spectral composition and inter-channel phase synchrony of the recorded ECoG signals. Heart cycle-related modulations of spectral power in the low-frequency range (up to approx. 12 Hz) were most prominent, but clearly extended also into the higher-frequency ranges (Figs. 9e, f).

These patterns were consistently observed over electrodes and patients. The spectral power changes were most striking especially in channels where high amplitude pulsatility artifacts were recorded. Heart cycle-related effects should thus be taken into account in spectral analysis of ECoG recordings up to high gamma frequencies.

Further, analysis of phase synchrony revealed that ECoG electrodes with pronounced pulsatility artifacts (e.g., Fig. 3b, IHC-4; Fig. 3c, G-F3) typically had a high phase synchrony index (PSI) with the ECG signal (e.g., Fig. 11a, white circles 1, 2) and also tended to show high PSIs between each other (e.g., Fig. 11a, white circle 4). As all these channels had pronounced pulsatility artifacts, it seems likely that the high PSIs among these channels are caused by these pulsatility artifacts. The observed "network" thus can be assumed to be a pulsatility-artifact-evoked phase synchrony pattern, rather than an indication of neuronal connectivity between brain signals. Additionally, neuronal activity in an extended network of areas supporting sensory processing and efferent control of cardiac activity may also have contributed to the observed connectivity pattern.

We applied a template correction in which we subtracted the averaged heart cycle-related potential from every single trial for each ECoG channel (see Materials and methods section for further details). After this correction, PSIs between the ECG signal and ECoG channels (Fig. 11b) as well as the strong PSIs among ECoG channels (e.g., F3 to IHC-4; Fig. 11b) decreased considerably. This shows that even a simple and straightforward template correction can successfully be applied to suppress "pseudo-connectivity" changes due to heart cycle-related effects (including both neuronal activity and artifact contamination) — which would be both unwanted and potentially confounding in many connectivity studies. Taking into account heart cycle-related phase-synchrony patterns in the ECoG would be especially important when investigating tasks changing the heart pulse rate of subjects. Such changes may result in real, transient connectivity changes, or they may reflect pseudo-changes, reflecting only artifact contaminations. Heart pulse rate changes occur, e.g., in cognitive tasks (Lacey, 1959; Lacey and Lacey, 1974, 1978; Morris and Thompson, 1969; Spence et al., 1972), emotional conditions (Critchley et al., 2005), as well as motor (Astrand and Saltin, 1961; Bergh et al., 1976) and motor imagery tasks (Beyer et al., 1990).

ECoG channels with low PSI to the ECG signal, but with high PSI between each other were hardly affected by the template correction (e.g., Fig. 11; white circles 6, 7). Hence, signals in these channels were either induced components of the recorded signals, i.e., not phase-locked to the heart cycle, or they were evoked (phase-locked) but with variable amplitudes, leaving an evoked residue after subtraction of the average response. This long-range phase synchronization might reflect true network characteristics from widely separated brain regions. However, further investigations in this direction are necessary to study the origin of this kind of apparent connectivity. Results of such studies might lead to an ECoG-based definition of the neural networks involved in processing cardiac-related signals.

Practical conclusions

Two basically different application scenarios need to be treated separately: (i) studies aimed at investigating the neural basis of sensory processing and viscero-motor control of the heart and (ii) studies interested in other functions. In the first case, only heart cycle-related artifacts are a problem and should be separated from heart cycle-related brain responses. In the second case, both heart cycle-related artifacts and brain responses may equally confound the effects of interest and should both be avoided or removed. The subtraction approach described above serves the second purpose, but not the first.

The impact and practical importance of heart cycle-related effects may be quite different, depending on the exact analysis approach. On the one hand, in the analysis of trial-averaged data in tasks without synchronization of the triggers used for analysis with the heartbeats, the impact of heart cycle-related effects may be quite small. In this case, heart cycle-related effects may just add some additional variance to the data, depending on the placement of electrodes and the frequency components investigated. Still, it may be useful to reduce such variance (noise). On the other hand, the present findings indicate that it can be of paramount importance to avoid heart cycle-related effects in the case of connectivity studies on tasks/conditions which have an impact on heart pulse rate. If not taken properly into account, heart cycle-related effects may induce pronounced, artificial connectivity patterns of their own, with little bearing on changes in brain activity. Therefore, as a practical conclusion, heart cycle-related effects should be carefully evaluated in studies on connectivity in intracranial EEG.

Nevertheless, the high spatial and temporal accuracy, together with the excellent overall signal quality of ECoG enabled, in the present study, the demonstration of an HEP with a stereotypical time course and topographical distribution that were both clearly and consistently observed over subjects. ECoG is, thus, a promising tool for the investigation of heartbeat-related viscerosensory processing in the human brain.

Acknowledgments

This work was supported by the BIAL Foundation grant 231/10 to Tonio Ball, and by the DFG grant EXC 1086 BrainLinks-BrainTools to the University of Freiburg, Germany.

Conflict of interest

The authors have no conflict of interest to declare.

Appendix A. Supplementary data

Supplementary data to this article can be found online at http://dx.doi.org/10.1016/j.neuroimage.2013.05.042.

References

Astrand, P.-O., Saltin, B., 1961. Maximal oxygen uptake and heart rate in various types of muscular activity. J. Appl. Physiol. 16, 977–981.
Ball, T., Nawrot, M.P., Pistohl, T., Aertsen, A., Schulze-bonhage, A., Mehring, C., 2004. Towards an implantable brain–machine interface based on epicortical field potentials. In: Biomedizinische Technik (Ed.), Biomedical Engineering, 38: Jahrestagung Der Deutschen Gesellschaft Für Biomedizinische Technik Im VDE — BMT 2004, pp. 756–759.
Ball, T., Demandt, E., Mutschler, I., Neitzel, E., Mehring, C., Vogt, K., Aertsen, Ad, Schulze-Bonhage, A., 2008. Movement related activity in the high gamma range of the human EEG. NeuroImage 41, 302–310.
Ball, T., Kern, M., Mutschler, I., Aertsen, Ad, Schulze-Bonhage, A., 2009. Signal quality of simultaneously recorded invasive and non-invasive EEG. NeuroImage 46, 708–716.
Ball, T., Schulze-Bonhage, A., Aertsen, Ad, Mehring, C., 2009. Differential representation of arm movement direction in relation to cortical anatomy and function. J. Neural Eng. 6, 016006.
Barlow, J.S., Dubinsky, J., 1980. EKG-artifact minimization in referential EEG recordings by computer subtraction. Electroencephalogr. Clin. Neurophysiol. 48, 470–472.
Bechara, A., Naqvi, N., 2004. Listening to your heart: interoceptive awareness as a gateway to feeling. Nat. Neurosci. 7, 102–103.
Benjamini, Y., Drai, D., Elmer, G., Kafkafi, N., Golani, I., 2001. Controlling the false discovery rate in behavior genetics research. Behav. Brain Res. 125, 279–284.
Bergh, U., Kanstrup, I.L., Ekblom, B., 1976. Maximal oxygen uptake during exercise with various combinations of arm and leg work. J. Appl. Physiol. 41, 191–196.
Beyer, L., Weiss, T., Hansen, E., Wolf, A., Seidel, A., 1990. Dynamics of central nervous activation during motor imagination. Int. J. Psychophysiol. 9, 75–80.
Binnie, C.D., 2003. Clinical Neurophysiology: EEG, Paediatric Neurophysiology, Special Techniques and Applications. Elsevier Health Sciences.
Bleichner, M.G., Vansteensel, M.J., Huiskamp, G.M., Hermes, D., Aarnoutse, E.J., Ferrier, C.H., Ramsey, N.F., 2011. The effects of blood vessels on electrocorticography. J. Neural Eng. 8, 044002.
Cameron, O.G., Minoshima, S., 2002. Regional brain activation due to pharmacologically induced adrenergic interoceptive stimulation in humans. Psychosom. Med. 64, 851–861.
Canolty, R.T., Edwards, E., Dalal, S.S., Soltani, M., Nagarajan, S.S., Kirsch, H.E., Berger, M.S., Barbaro, N.M., Knight, R.T., 2006. High gamma power is phase-locked to theta oscillations in human neocortex. Science 313, 1626–1628.

Canolty, R.T., Soltani, Maryam, Dalal, Sarang S., Edwards, Erik, Dronkers, N.F., Nagarajan, Srikantan S., Kirsch, Heidi E., Barbaro, Nicholas M., Knight, Robert T., 2007. Spatiotemporal dynamics of word processing in the human brain. Front. Neurosci. 1, 1.

Chang, C., Cunningham, J.P., Glover, G.H., 2009. Influence of heart rate on the BOLD signal: the cardiac response function. NeuroImage 44, 857–869.

Cooper, N.R., Croft, R.J., Dominey, S.J.J., Burgess, A.P., Gruzelier, J.H., 2003. Paradox lost? Exploring the role of alpha oscillations during externally vs. internally directed attention and the implications for idling and inhibition hypotheses. Int. J. Psychophysiol. 47, 65–74.

Cooper, R., Binnie, C.D., Osselton, J.W., Prior, P.F., Wisman, T., 2003. EEG technology. Clinical Neurophysiology: EEG, Paediatric Neurophysiology, Special Techniques and Applications. Elsevier Health Sciences, pp. 8–103.

Critchley, H.D., Wiens, S., Rotshtein, P., Ohman, A., Dolan, R.J., 2004. Neural systems supporting interoceptive awareness. Nat. Neurosci. 7, 189–195.

Critchley, H.D., Rotshtein, P., Nagai, Y., O'Doherty, J., Mathias, C.J., Dolan, R.J., 2005. Activity in the human brain predicting differential heart rate responses to emotional facial expressions. NeuroImage 24, 751–762.

Crone, N.E., Miglioretti, D.L., Gordon, B., Lesser, R.P., 1998. Functional mapping of human sensorimotor cortex with electrocorticographic spectral analysis. II. Event-related synchronization in the gamma band. Brain 121, 2301–2315.

Crone, N.E., Miglioretti, D.L., Gordon, B., Sieracki, J.M., Wilson, M.T., Uematsu, S., Lesser, R.P., 1998. Functional mapping of human sensorimotor cortex with electrocorticographic spectral analysis. I. Alpha and beta event-related desynchronization. Brain 121 (Pt. 12), 2271–2299.

Crone, N.E., Sinai, A., Korzeniewska, A., 2006. High-frequency gamma oscillations and human brain mapping with electrocorticography. Event-Related Dynamics of Brain Oscillations. Elsevier, pp. 275–295.

Dirlich, G., Vogl, L., Plaschke, M., Strian, F., 1997. Cardiac field effects on the EEG. Electroencephalogr. Clin. Neurophysiol. 102, 307–315.

Dirlich, G., Dietl, T., Vogl, L., Strian, F., 1998. Topography and morphology of heart action-related EEG potentials. Electroencephalogr. Clin. Neurophysiol. 108, 299–305.

Dworetzky, B., Herman, S., Tatum, W.O., 2010. Artifacts of recording. In: Niedermeyer, E., da Silva, F.L. (Eds.), Electroencephalography: Basic Principles, Clinical Applications, and Related Fields. Lippincott Williams & Wilkins, Philadelphia, pp. 239–266.

Engel, A.K., Moll, C.K.E., Fried, I., Ojemann, G.A., 2005. Invasive recordings from the human brain: clinical insights and beyond. Nat. Rev. Neurosci. 6, 35–47.

Enzmann, D.R., Pelc, N.J., 1992. Brain motion: measurement with phase-contrast MR imaging. Radiology 185, 653–660.

Fukushima, H., Terasawa, Y., Umeda, S., 2011. Association between interoception and empathy: evidence from heartbeat-evoked brain potential. Int. J. Psychophysiol. 79, 259–265.

Gray, M.A., Taggart, P., Sutton, P.M., Groves, D., Holdright, D.R., Bradbury, D., Brull, D., Critchley, H.D., 2007. A cortical potential reflecting cardiac function. Proc. Natl. Acad. Sci. U. S. A. 104, 6818–6823.

Greitz, D., Wirestam, R., Franck, A., Nordell, B., Thomsen, C., Ståhlberg, F., 1992. Pulsatile brain movement and associated hydrodynamics studied by magnetic resonance phase imaging. The Monro–Kellie doctrine revisited. Neuroradiology 34, 370–380.

Handy, T.C., 2004. Event-Related Potentials: a Methods Handbook. MIT Press.

Hirsch, L., Brenner, R., 2010. Atlas of EEG in Critical Care, 1. Auflage. John Wiley & Sons.

Jerbi, K., Freyermuth, S., Dalal, S., Kahane, Philippe, Bertrand, O., Berthoz, A., Lachaux, J.-P., 2009. Saccade related gamma-band activity in intracerebral EEG: dissociating neural from ocular muscle activity. Brain Topogr. 22, 18–23.

Khalsa, S.S., Rudrauf, D., Feinstein, J.S., Tranel, D., 2009. The pathways of interoceptive awareness. Nat. Neurosci. 12, 1494–1496.

Kovach, C.K., Tsuchiya, N., Kawasaki, H., Oya, H., Howard III, M.A., Adolphs, R., 2011. Manifestation of ocular-muscle EMG contamination in human intracranial recordings. NeuroImage 54, 213–233.

Lacey, J.I., 1959. Psychophysiological approaches to the evaluation of psychotherapeutic process and outcome. In: Rubinstein, E.A., Parloff, M.B. (Eds.), Research in Psychotherapy. American Psychological Association, Washington, DC, US, pp. 160–208.

Lacey, B.C., Lacey, J.I., 1974. Studies of heart rate and other bodily processes in sensorimotor behavior. In: Obrist, P.A., Black, A.H., Brener, J., DiCara, L.V. (Eds.), Cardiovascular Psychophysiology: Current Issues in Response Mechanisms, Biofeedback and Methodology. AldineTransaction, New Brunswick, NJ, US, pp. 538–564.

Lacey, B.C., Lacey, J.I., 1978. Two-way communication between the heart and the brain. Significance of time within the cardiac cycle. Am. Psychol. 33, 99–113.

Lachaux, J.P., Rodriguez, E., Martinerie, J., Varela, F.J., 1999. Measuring phase synchrony in brain signals. Hum. Brain Mapp. 8, 194–208.

Lachaux, J.P., Rudrauf, D., Kahane, P., 2003. Intracranial EEG and human brain mapping. J. Physiol. Paris 97, 613–628.

Lachaux, J.P., George, N., Tallon-Baudry, C., Martinerie, J., Hugueville, L., Minotti, L., Kahane, P., Renault, B., 2005. The many faces of the gamma band response to complex visual stimuli. NeuroImage 25, 491–501.

Leopold, C., Schandry, R., 2001. The heartbeat-evoked brain potential in patients suffering from diabetic neuropathy and in healthy control persons. Clin. Neurophysiol. 112, 674–682.

Leuthardt, E.C., Schalk, G., Wolpaw, J.R., Ojemann, J.G., Moran, D.W., 2004. A brain–computer interface using electrocorticographic signals in humans. J. Neural Eng. 1, 63–71.

Miller, K.J., Sorensen, L.B., Ojemann, J.G., den Nijs, M., 2009. Power-law scaling in the brain surface electric potential. PLoS Comput. Biol. 5.

Misra, 2005. Clinical Electroencephalography. Elsevier, India.

Montoya, P., Schandry, R., Müller, A., 1993. Heartbeat evoked potentials (HEP): topography and influence of cardiac awareness and focus of attention. Electroencephalogr. Clin. Neurophysiol. 88, 163–172.

Morris, J.D., Thompson, L.W., 1969. Heart rate changes in a reaction time experiment with young and aged subjects. J. Gerontol. 24, 269–275.

Otsubo, H., Ochi, A., Imai, K., Akiyama, T., Fujimoto, A., Go, C., Dirks, P., Donner, E.J., 2008. High-frequency oscillations of ictal muscle activity and epileptogenic discharges on intracranial EEG in a temporal lobe epilepsy patient. Clin. Neurophysiol. 119, 862–868.

Panagiotides, H., Freeman, W.J., Holmes, M.D., Pantazis, D., 2011. Behavioral states may be associated with distinct spatial patterns in electrocorticogram. Cogn. Neurodyn. 5, 55–66.

Percival, D., 2000. Wavelet Methods for Time Series Analysis. Cambridge University Press, Cambridge; New York.

Pérez, J.J., Guijarro, E., Barcia, J.A., 2005. Suppression of the cardiac electric field artifact from the heart action evoked potential. Med. Biol. Eng. Comput. 43, 572–581.

Pistohl, T., Schulze-Bonhage, A., Aertsen, A., Mehring, C., Ball, T., 2012. Decoding natural grasp types from human ECoG. NeuroImage 59, 248–260.

Pollatos, O., Schandry, R., 2004. Accuracy of heartbeat perception is reflected in the amplitude of the heartbeat-evoked brain potential. Psychophysiology 41, 476–482.

Pollatos, O., Kirsch, W., Schandry, R., 2005. Brain structures involved in interoceptive awareness and cardioafferent signal processing: a dipole source localization study. Hum. Brain Mapp. 26, 54–64.

Pollatos, O., Schandry, R., Auer, D.P., Kaufmann, C., 2007. Brain structures mediating cardiovascular arousal and interoceptive awareness. Brain Res. 1141, 178–187.

Schalk, G., Kubánek, J., Miller, K.J., Anderson, N.R., Leuthardt, E.C., Ojemann, J.G., Limbrick, D., Moran, D., Gerhardt, L.A., Wolpaw, J.R., 2007. Decoding two-dimensional movement trajectories using electrocorticographic signals in humans. J. Neural Eng. 4, 264–275.

Schalk, G., Leuthardt, E.C., Brunner, P., Ojemann, J.G., Gerhardt, L.A., Wolpaw, J.R., 2008. Real-time detection of event-related brain activity. NeuroImage 43, 245–249.

Schandry, R., Montoya, P., 1996. Event-related brain potentials and the processing of cardiac activity. Biol. Psychol. 42, 75–85.

Schandry, R., Weitkunat, R., 1990. Enhancement of heartbeat-related brain potentials through cardiac awareness training. Int. J. Neurosci. 53, 243–253.

Schandry, R., Sparrer, B., Weitkunat, R., 1986. From the heart to the brain: a study of heartbeat contingent scalp potentials. Int. J. Neurosci. 30, 261–275.

Schroth, G., Klose, U., 1992. Cerebrospinal fluid flow I. Physiology of cardiac-related pulsation. Neuroradiology 35, 1–9.

Schroth, G., Klose, U., 1992. Cerebrospinal fluid flow. III. Pathological cerebrospinal fluid pulsations. Neuroradiology 35, 16–24.

Shao, S., Shen, K., Wilder-Smith, E.P.V., Li, X., 2011. Effect of pain perception on the heartbeat evoked potential. Clin. Neurophysiol. 122, 1838–1845.

Shimoda, K., Nagasaka, Y., Chao, Z.C., Fujii, N., 2012. Decoding continuous three-dimensional hand trajectories from epidural electrocorticographic signals in Japanese macaques. J. Neural Eng. 9, 036015.

Sinai, A., Bowers, C.W., Crainiceanu, C.M., Boatman, D., Gordon, B., Lesser, R.P., Lenz, F.A., Crone, N.E., 2005. Electrocorticographic high gamma activity versus electrical cortical stimulation mapping of naming. Brain 128, 1556–1570.

Spence, D.P., Lugo, M., Youdin, R., 1972. Cardiac change as a function of attention to and awareness of continuous verbal text. Science 176, 1344–1346.

Stern, J.M., 2004. Atlas of EEG Patterns. Lippincott Williams & Wilkins.

Tracy, J., Goyal, N., Flanders, A., Weening, R., Laskas, J., Natale, P., Waldron, B., 2007. Functional magnetic resonance imaging analysis of attention to one's heartbeat. Psychosom. Med. 69, 952–960.

Wagshul, M.E., Eide, P.K., Madsen, J.R., 2011. The pulsating brain: a review of experimental and clinical studies of intracranial pulsatility. Fluids Barriers CNS 8, 5.

Yuan, H., Yan, H.-M., Xu, X.-G., Han, F., Yan, Q., 2007. Effect of heartbeat perception on heartbeat evoked potential waves. Neurosci. Bull. 23, 357–362.

Zumsteg, D., Hungerbühler, H., Wieser, H.-G., 2004. Atlas of Adult Electroencephalography, First ed. Hippocampus.